Supporting Information

Su et al. 10.1073/pnas.1013592107

SI Text

Identification of Antiinfluenza Hits by High-Throughput Screening of a Large Compound Library. For high-throughput screening (HTS) screening of a large number of compounds, the time and costs are critical factors for screening designs. We chose to use 1,536-well microplates to screen a large chemical library to reduce both the cost and screening times. Thus, we could not use the reported procedure for antiinfluenza screening using 384-well plates (1, 2). In general, simple screening protocols are preferred for faster method development and lower costs, particularly for 1,536-well assay platforms. We used cytopathic effects (CPE) protection as the principle for antiinfluenza inhibitor screening. The CPE protection can be measured in a cost-effective manner based on the cellular ATP contents determined using a luminescence reporting system. The criteria for our antiinfluenza HTS assay development were set to achieve (1) uniform luminescence signals from MDCK cells in all wells, (2) significant and uniform reduction in luminescence signals due to influenza infection mediated CPE, and (3) demonstration of luminescence signal increase using a model antiinfluenza drug. The above criteria were met in our assay development in 1,536-well plates by optimizing MDCK cell number, multiplication of infection, and infection times. An example of the optimized assay result is shown in Fig. S1. In the "cell only" wells in Fig. S1*A*, equal volumes of MDCK cell suspension were pumped into each well. Three days later, the live cell densities, measured by the luminescence signals, were uniform. Similarly, MDCK cells in wells infected with WSN (H1N1) also resulted in uniform CPE shown as low luminescence signals. To demonstrate that CPE protection could be used for the identification of active antiinfluenza agents, Oseltamivir carboxylate (OC) at varied concentrations were added to WSN infected MDCK cells and resulted in dose-dependent protection of the influenza mediated CPE effects. The image of Fig. 1*A* was digitized and shown as a scatter plot (Fig. S1*B*). The signals of uninfected and the infected cells are both uniform with %CV values of 11% and 17%, respectively. In addition, the signals of these two groups are well separated with a Z' value of 0.6, indicating that the signal-to-noise ratio is adequate for an HTS assay. The signals of wells containing infected MDCK cells and those treated with OC at 1,875 or 188 nM are also well separated from the signals of untreated infected cells. Treatments with 19 nM OC resulted in smaller CPE protections, but most wells had greater signals than those of untreated cells. These results suggest that our HTS protocol most likely will not miss inhibitors with greater antiinfluenza activities as OC at 19 nM. It is noted that the EC_{50} value of OC measured in comparable conditions against WSN is about 30 nM.

Fig. S1*C* is a histogram summarizing the activity distribution of all assay samples. A small population of assay samples was found to have greater CPE protection activities, suggesting that our HTS campaign can identify a minor population of hit compounds that protect the influenza mediated CPE. Preliminary analysis of some of these hits led to the understanding that many of these CPE protective hits do not inhibit influenza replications. This finding suggested that it is necessary to rule out false positive hits by further screening the hits for antiinfluenza inhibitors. For antiviral activities, viral yield reduction assays are more reliable for evaluating the inhibitory effects on viral replication and are usually done by counting viral plaques, a time-consuming low throughput process. We developed a platform called "Microplate Counting for Infectious Particles" (McIP) that is based on the automated counting of viral antigen expressing fluorescence cells to determine the infectious particles using 96-well plates. Fig. S2 shows that the enumeration of the infectious influenza particles by McIP results in a comparable measurement as the pfu (plaque forming unit) determination method using agar overlays (3, 4). All HTS hits confirmed to protect the influenza mediated CPE at 5 μM were used to treat 10^4 MDCK cells infected with 300 infectious WSN influenza viruses per well. At 24 h post infection, the conditioned media of the infected cells were harvested, diluted, and used to determine the influenza yields by infecting fresh MDCK cells to determine the number of infectious particles that are shown as fluorescent cells expressing influenza nuclear protein (NP) antigen. The number of infected cells was enumerated in an automated manner allowing the determination of viral yields in high throughput. The viral yield reduction by treatment using several representative antiinfluenza hits indicates that these compounds inhibited A/WSN/1933/(H1N1) replication during the 24 h treatments.

Among the confirmed inhibitory hits for WSN, antiinfluenza drugs such as Oseltamivir carboxylate, and Zanamivir were identified by the screening of the compound library. Two other hits, Monensin and Nigercin are known ionophore inhibitors interfering with the endosomal-lysosomal acidification and vesicular trafficking (5–7) and have been reported to inhibit a wide range of viruses (8, 9). The structures of the four established antiinfluenza compounds are shown in Fig. S3.

Characterization of the New Antiinfluenza Compounds Identified by HTS. We attempted to select for inhibitor-resistant mutants using the new antiinfluenza compounds to explore if they are targeting the influenza encoded genes. We were successful in identifying resistant mutants by serial passages of WSN viruses in three of the four inhibitors. Therefore as shown in Fig. S4, compounds **788** (Nucleozin), **367**, and **1075** are probably inhibiting WSN virus by targeting the viral genes. To try to identify the **3061** (FA-2) targets, seven strains of **3061** (FA-2)-resistant WSN mutants (Fig. S4*E*) were obtained by selection using **788** (Nucleozin) or **3061** (FA-2).

Antiinfluenza Properties of the 788 (Nucleozin) Analogs with Substituted Isoxazolyl Carbonyl Piperazine Structures. Fig. S5 shows that **3061** (FA-2) is also active in inhibiting the replication of clinical isolates of H1N1 collected in Taiwan before 2009. There are both Oseltamivir resistant and susceptible H1N1 strains, and **3061** (FA-2) treatments are effective in reducing the WSN yields in MDCK cells after a one day infection. Our virus challenge studies also confirmed that **3061** (FA-2) can partially protect mice from virus-induced mortality (Fig. S6). Sequencing analysis of the seven mutants as well as cell-based studies suggested that **3061** (FA-2) targets NP protein and that the viruses carrying the mutation Y289H or Y52H on NP are resistant to **3061** (Table 2 and Fig. S7). As shown in Fig. S8*A*, incubation of recombinant NP proteins with **788** (Nucleozin) or **3061** would cause NP aggregation from the original trimeric forms. It was predicted that **788** (Nucleozin) or **3061** (FA-2) may insert between the residues R99 and Y52 or Y52 and Y313, to disrupt the loop stability, leading to the aggregation of NP proteins (Fig. S8*B*). Neither Y52H nor Y289H would affect the replication of viruses because recombinant viruses in WSN background carrying Y52H or Y289H or both mutations can grow well on MDCK cells (Fig. S9).

SI Materials and Methods. ***High-throughput screening.*** HTS studies were performed at the Genomics Research Center of Academia

Sinica in Taiwan using the uHTS system manufactured by GNF systems (San Diego, CA). Libraries's compounds were collected from local laboratories and purchased from different vendors, such as ChemDiv (San Diego, CA, USA), ChemBridge (San Diego, CA, USA), Life Chemicals (Kiev, Ukraine), and AMRI (Budapest, Hungary). Compounds were prepared at 1 mM in 100% DMSO in 1,536-well propylene plates and stored online in the HTS system. The antiflu activities of the compound collection were conducted by the protection of the influenza virus mediated cytopathic activities. About 500 MDCK cells were seeded onto the wells of 1,536-well plates at 4 μL/well in infection medium (DMEM, 2% FBS). After an overnight incubation in the environmentally controlled incubators (35 °C, 5% CO_2, 100% humidity), the cells were added with compounds using a 1,536-pin transfer device with 50 nL pins (V&P Scientific) followed by infection with 480 pfu of H1N1 influenza virus (WSN33) per well of a 1,536-well plates. The plates were further incubated in the environmentally controlled incubators (35 °C, 5% CO_2, 100% humidity) for 3 d. The CPE were determined with Cell-Titer Glo® (Promega) and the luminescence was monitored with the Perkin-Elmer Viewlux.

Assay development and data analysis for enumeration of the infectious particles by McIP. Ten thousand MDCK cells were seeded onto the wells of 96-well black-clear-bottom plates (Packard) one day prior to infection. One hundred μL of infection medium (2% FBS in DMEM) containing influenza virus WSN33 in various pfus were added to MDCK cells followed with a 17-h incubation at 37 °C unless stated otherwise. After washing with phosphate-buffered saline (PBS, pH 7.4), cells were fixed with methanol for 3 min, blocked with 5% nonfat milk in PBS for 1 h, washed again with PBS, and then incubated with anti-NP antibodies diluted 1:4,000 in 0.5% nonfat milk in PBS for another hour. After three washes with PBS, cells were further incubated with fluorescein-conjugated secondary antibodies diluted 1:2,000 in PBS with 0.5% nonfat milk for one hour. Alternatively, anti-WSN33 rabbit antiserum diluted 1:500 in PBS with 0.5% nonfat milk was used as the first antibodies for comparison. The plates were then scanned with the Isocyte™ laser scanning platform (Molecular Device) with a single-channel of acquisition. Fluorescein fluorescence was captured using a 510- to 540-nm band pass filter upon a 488-nm laser excitation. The entire 96-well plate was scanned at 5×5 μm^2 sampling with acquisition of a complete image of each well.

The images of wells were processed using the proprietary software BlueImage (10) to determine the number of fluorescent particles. Briefly, a circular region of interest that covers the whole well was predefined in the image. A "rolling ball" flattening algorithm with a characteristic width of 300 μm, and an area filter for 3,000 μm^2 and above were employed. To find an optimized threshold value, the threshold was initially set to a constant between 500 ~ 1,000 to determine the particle number of influenza sample used to infect MDCK cells. The region of interest was set to cover the entire well, including the particles detected on the boundary. To exclude background noises, an area filter to include particles ranging from 3,000 ~ 50,000 μm^2 in size and a threshold filter for fluorescence intensity above 1,000 were applied. These settings gave us the closest representation of fluorescence particle numbers and smallest standard deviations. The threshold at which the obtained count particles was the closest to the expected plaque forming unit of the control was then applied for analysis. The result from each well was processed and analyzed using the same parameters during image acquisition. Plate results were recorded on a well-by-well basis in a text file and exported to Prism (GraphPad Software) for further analysis.

High-throughput viral yield assay for antiviral agents. Primary hits identified from HTS were picked with the hit-picker system (GNF systems) and were used for confirmation with viral yield assay using 96-well plates. Ten thousand MDCK cells were plated onto the wells of 96-well plates one day prior to incubation with the tested molecules at various concentrations, immediately followed by an infection with 300 pfu of WSN viruses in 100 μL of infection medium. The cell media containing progeny viruses were collected at 24 h post infection, diluted in 100-fold in the infection medium, and added to MDCK cells in the wells of a 96-well plate. After incubation for 17 h at 37 °C, the cells were processed for enumeration of infected particles as described above. For each 96-well assay plate, column 12 was left for positive controls (3 μM of Oseltamivir carboxylate) and negative controls. The Z' value was calculated from the control wells and found to be above 0.8.

Protection of WSN infected mice by antiinfluenza inhibitor 3061 (FA-2). Antiinfluenza inhibitor compound **3061** (FA-2) was dissolved in dimethylacetamide and polyethylene glycol 400 and further diluted with PBS to 0.5 mg/mL. Eight week old Balb/c mice were grouped into 10 mice per group and used for the study. The compound was injected by intraperitoneal route once per day at 2.5 mg/kg for five days beginning on the day of WSN infection with WSN virus at 10 LD_{50} (50% Lethal Dose). Two controls of vehicle only and the 5 mg/kg Oseltamivir Carboxylate treated groups were included in the study. Mouse survival was observed daily and analyzed using Logrank test (Prism Graphpad).

Preparation of recombinant NP proteins using transfected E. coli cells. The cDNA sequences for the parental 52Y and the mutant 52H NP were cloned into pET28a and isolated as $(His)_6$ fusion proteins and isolated according to the procedures suggested by the manufacturer (Novagen Corp).

Analytical ultracentrifuge studies. Sedimentation velocity (SV) experiment was performed by a Beckman-Coulter XL-I analytical ultracentrifuge. Samples and buffers were loaded into 12 mm standard double-sector Epon charcoal-filled centerpieces and mounted in an An-60 Ti or An-50 Ti rotors. SV experiments were performed at rotor speed of 40,000 rpm at 20 °C, and monitored at 280 nm. The raw data were calculated using SedFit developed by Dynamics of Macromolecular Assembly group of the Laboratory of Bioengineering and Physical Science (DMA/LBPS), National Institute of Bioimaging and Bioengineering, NIH (11). The density and viscosity of buffer were calculated using Sednterp software (12). The partial specific volume of influenza A NP is 0.7256. All samples were visually checked for clarity after ultracentrifugation, and no precipitation was observed.

Differential distribution of sedimentation coefficients and fictional ratios $c(s,fr)$ were calculated with Sedfit using $c(s,*)$ model with Eq. **1** (13).

$$a(r{\cdot}t) = \iint c(s,fr) \times (s,D(s,fr),r,t)dsdfr. \qquad \textbf{[S1]}$$

The $c(s,fr)$ distribution could be transformed to a molar mass distribution for each s-value, called $c(s,M)$ distribution, by Eq. **2** (13).

$$a(r,t) = \iint c(s,M) \times (s,D(s,M)r,t)dsdM \qquad \textbf{[S2]}$$

Modeling of NP and interaction prediction with 3061 (FA-2). The molecular complex of compound **3061** (FA-2) and NP of influenza A virus was modeled by an induced fit docking method of Glide™ (Schrödinger). The X-ray structure of NP was downloaded from RCSB Protein Data Bank (PDB coded 2iqh) (14). The protein

structure was first added hydrogen atoms and was then refined using Macromodel™ (Schrödinger). In docking process, protein side chains Y52, R99, and Y313 were allowed to be flexible, and the van der Waals scaling factor was set to 0.7 with a cutoff of 0.25 Å. Compound **3061** (FA-2) was first docked in SP (standard precision) mode of Glid™ with the van der Waals scaling factor of the compound set to 0.5 and a cutoff of 0.15 Å. This initial binding model was further refined using XP (extra precision) mode by setting the van der Waals scaling of the compound to 0.8 with a cutoff of 0.15 Å. In the final step, residues within 5 Å of the docked compound were further refined to optimize their interaction with the complex.

1. Noah JW, et al. (2007) A cell-based luminescence assay is effective for high-throughput screening of potential influenza antivirals. *Antiviral Res* 73:50–59.
2. Severson WE, et al. (2008) High-throughput screening of a 100,000-compound library for inhibitors of influenza A virus (H3N2). *J Biomol Screen* 13:879–887.
3. Appleyard G, Maber HB (1975) A plaque assay for the study of influenza virus inhibitors. *J Antimicrob Chemother* 1:49–53.
4. Palese P, Tobita K, Ueda M, Compans RW (1974) Characterization of temperature sensitive influenza virus mutants defective in neuraminidase. *Virology* 61:397–410.
5. Misinzo G, Delputte PL, Lefebvre DJ, Nauwynck HJ (2008) Increased yield of porcine circovirus-2 by a combined treatment of PK-15 cells with interferon-gamma and inhibitors of endosomal-lysosomal system acidification. *Arch Virol* 153:337–342.
6. Adachi K, et al. (2007) Inhibition of betanodavirus infection by inhibitors of endosomal acidification. *Arch Virol* 152:2217–2224.
7. Daniels PU, Edwardson JM (1988) Intracellular processing and transport of influenza-virus envelope proteins in Madin-Darby canine kidney cells. Effects of the carboxylic ionophores monensin and nigericin. *Biochem J* 252:693–700.
8. Sakaguchi T, Leser GP, Lamb RA (1996) The ion channel activity of the influenza virus M2 protein affects transport through the Golgi apparatus. *J Cell Biol* 133:733–747.
9. Pietropaolo V, Degener AM, Di Taranto C, Sinibaldi L, Orsi N (1995) The in vitro effect of monensin on BK polyomavirus replication. *New Microbiol* 18:341–349.
10. Lee PH, Miller SC, van Staden C, Cromwell EF (2008) Development of a homogeneous high-throughput live-cell G-protein-coupled receptor binding assay. *J Biomol Screen* 13:748–754.
11. Lebowitz J, Lewis MS, Schuck P (2002) Modern analytical ultracentrifugation in protein science: a tutorial review. *Prot Sci* 11:2067–2079.
12. Howlett GJ, Minton AP, Rivas G (2006) Analytical ultracentrifugation for the study of protein association and assembly. *Curr Opin Chem Biol* 10:430–436.
13. Brown PH, Schuck P (2006) Macromolecular size-and-shape distributions by sedimentation velocity analytical ultracentrifugation. *Biophys J* 90:4651–4661.
14. Ye Q, Krug RM, Tao YJ (2006) The mechanism by which influenza A virus nucleoprotein forms oligomers and binds RNA. *Nature* 444:1078–1082.

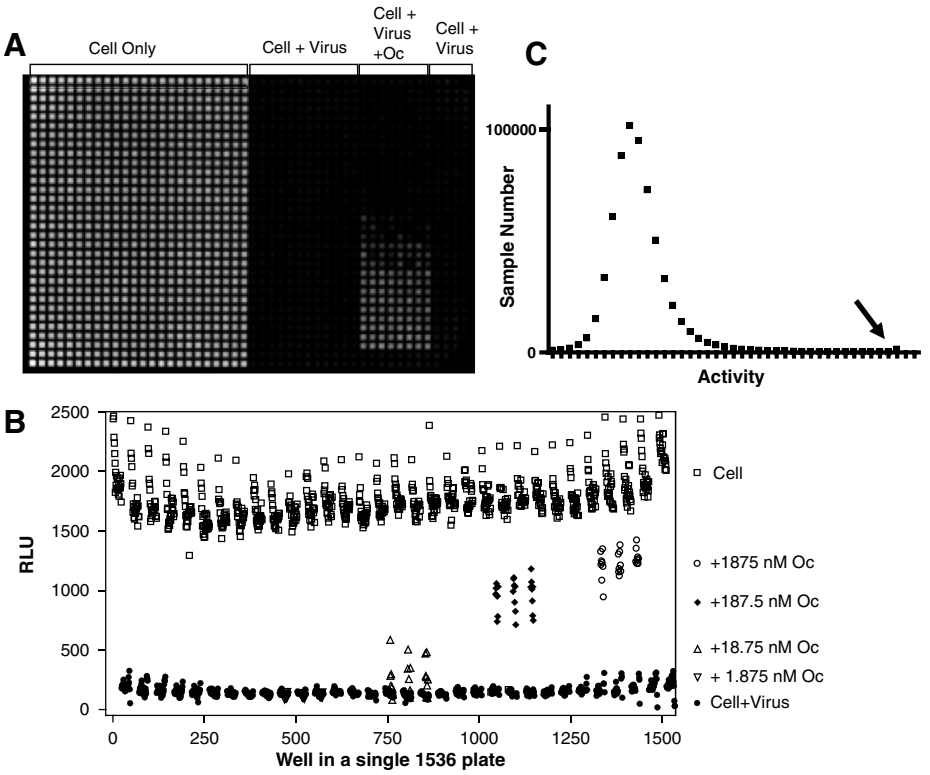

Fig. S1. Antiinfluenza HTS assay development and the profile of hits distribution. (*A*) Viability image of cells in a 1,536-well micro-plate with optimized assay conditions consisting of controls of uninfected, WSN infected MDCK cells, and infected cells treated with varied concentrations of OC demonstrating dose-dependent CPE protection with this reference inhibitor. (*B*) Scatter plot of relative luminescence values measuring the viabilities of cells treated under different assay conditions demonstrating well separated signals of different treatment groups. (*C*) Histogram of the HTS screening results summarizing the activity distribution of 631,552 samples. An arrow pointing at the small group of samples with highest CPE protection and were identified as hits in this HTS campaign.

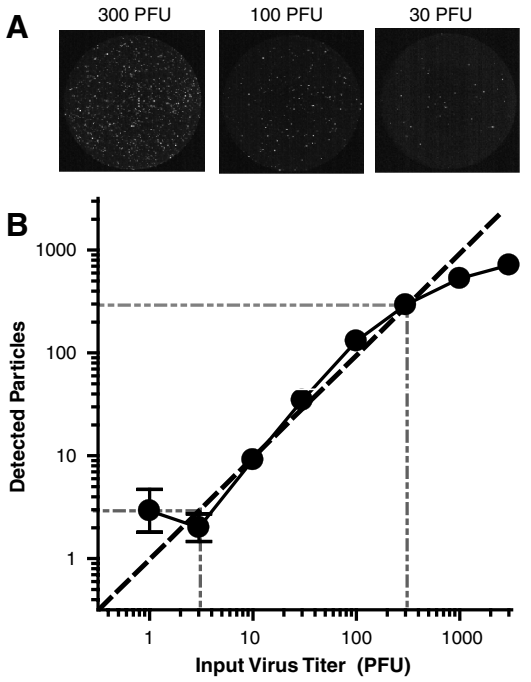

Fig. S2. Automated enumeration of infectious influenza particles by image analysis of infected cells in 96-wells and comparison with viral titer determination using traditional pfu assays. (*A*) Images of MDCK cells infected with 300, 100, and 30 pfu of WSN viruses in 96-wells, (*B*) Comparison of enumeration values determined by the McIP and the pfu determination by counting plaques after staining using the conventional agar overlay method.

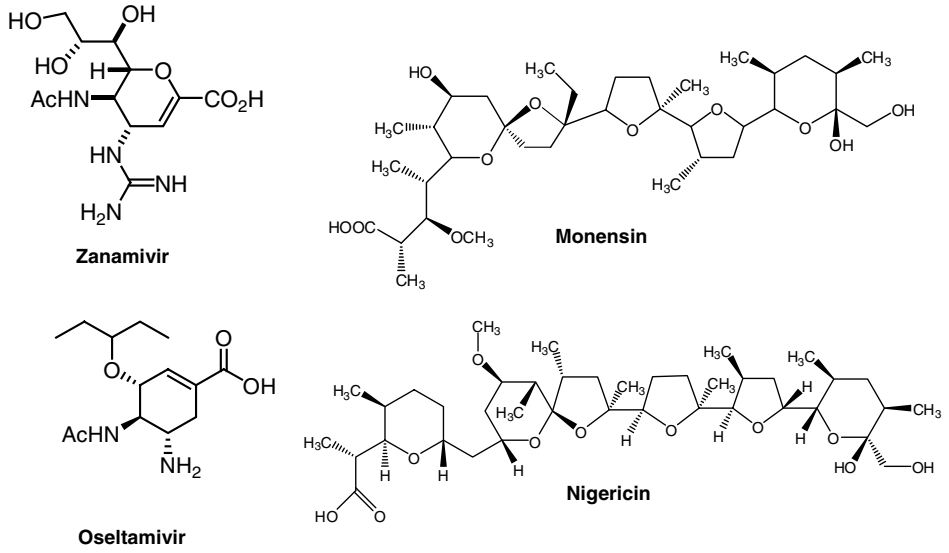

Fig. S3. Structures of known antiinfluenza inhibitors identified by HTS.

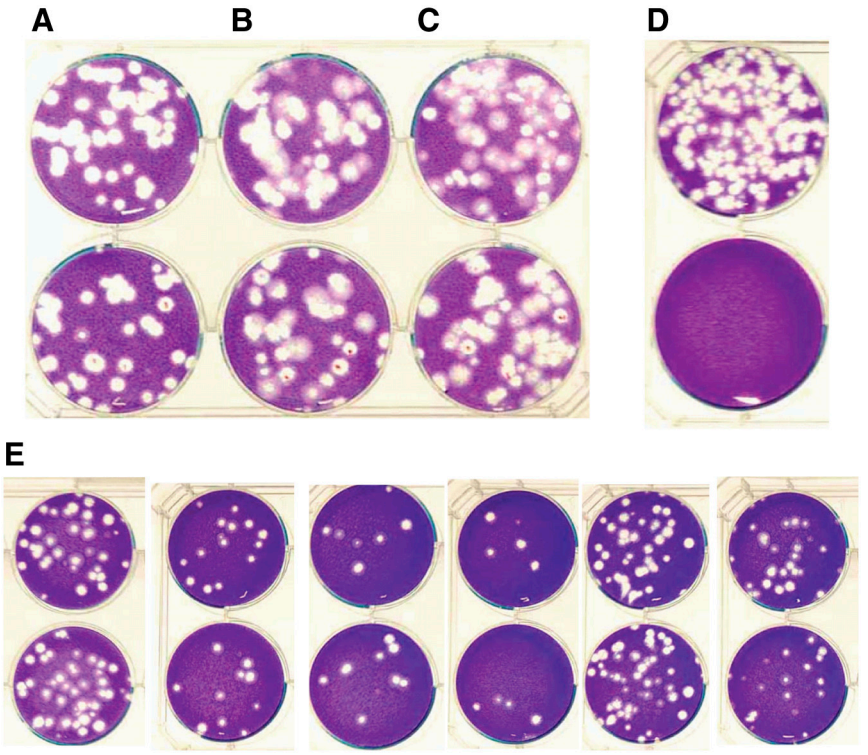

Fig. S4. Selection of antiinfluenza inhibitor-resistant WSN variants. Inhibitor-resistant WSN variants were selected that are fit with or without the presence of inhibitors in agar. (*A*) Growth of **788** (Nucleozin)-selected WSN variant on agar without inhibitor (top) and with 3 μM **3061** (FA-2) (bottom). (*B*) **1075**-selected variant in the absence of inhibitor (top) and with 10 μM **1075** (bottom). (*C*) **367**-selected variant on agar without inhibitor (top) and with 30 μM **367** (bottom). (*D*) Growth of parental WSN on agar without **3061** (FA-2) (top) and with 3 μM **3061** (FA-2) (bottom). (*E*) Growth of six **3061** (FA-2)-selected variants in the absence of 3061 (FA-2) (top) and with 3 μM **3061** (FA-2) (bottom).

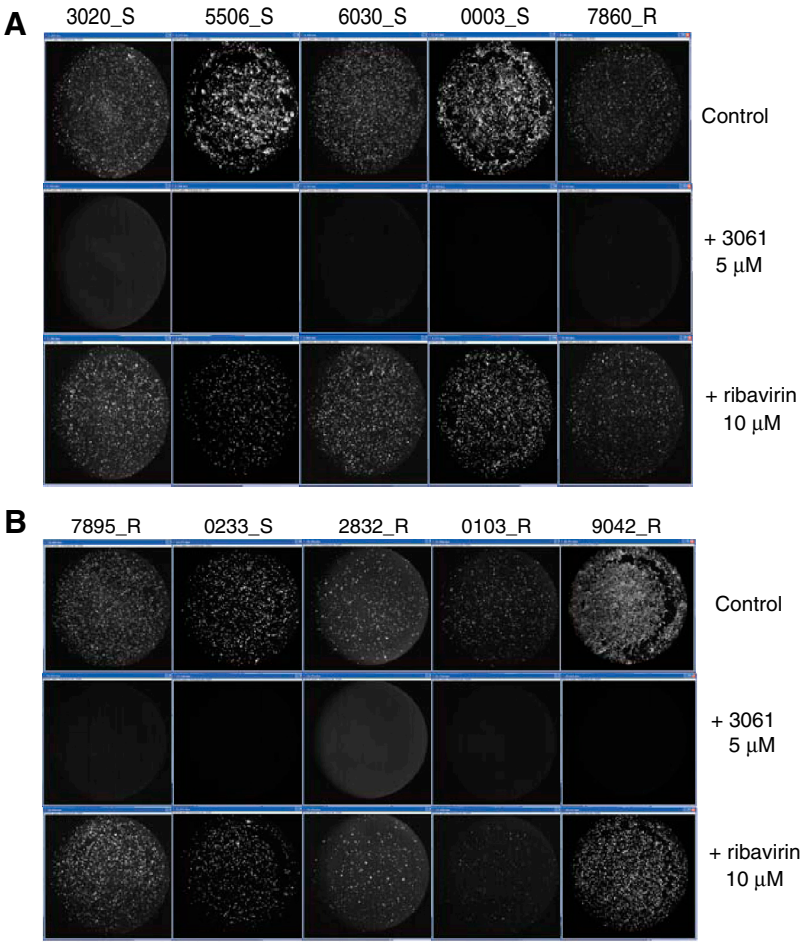

Fig. S5. (*A* and *B*) Ten clinical H1N1 strains isolated before 2009 in Taiwan that are either susceptible or resistant to Oseltamivir are sensitive to 5 μM **3061** (FA-2) in viral yield reduction assays, while ribavirin at 10 μM fails to reduce viral yields. The strain names suffixed with "S" or "R" indicate the susceptibility of the viruses to Oseltamivir. The experiments and procedures to generate the images are described in *SI Materials and Methods*.

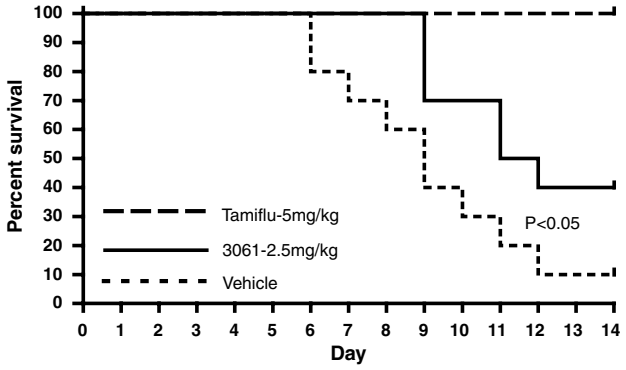

Fig. S6. Protection of H1N1 infected mice with **3061** (FA-2) treatments. Eight week old Balb/c mice were infected with WSN viruses, divided into 3 treatment groups, and injected by IP for 5 d with vehicle, 2.5 mg/kg **3061** (FA-2) or 5 mg/kg Tamiflu starting on the day of virus infection. During the 14 observation days all Tamiflu treated mice were protected. The group receiving 2.5 mg/kg **3061** (FA-2) was partially protected with $P < 0.05$ in comparison with the vehicle treatment group.

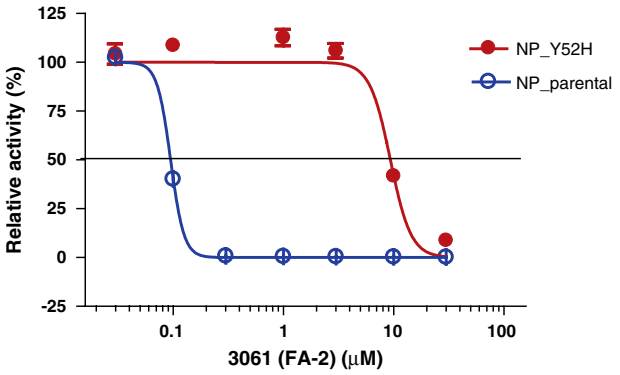

Fig. S7. Relative RdRP activity using NP-parental or NP_Y52H in the presence of different concentration of **3061** (FA-2). The fitting curves were generated using Prism (Graphpad) and the horizontal line indicated the 50% inhibition.

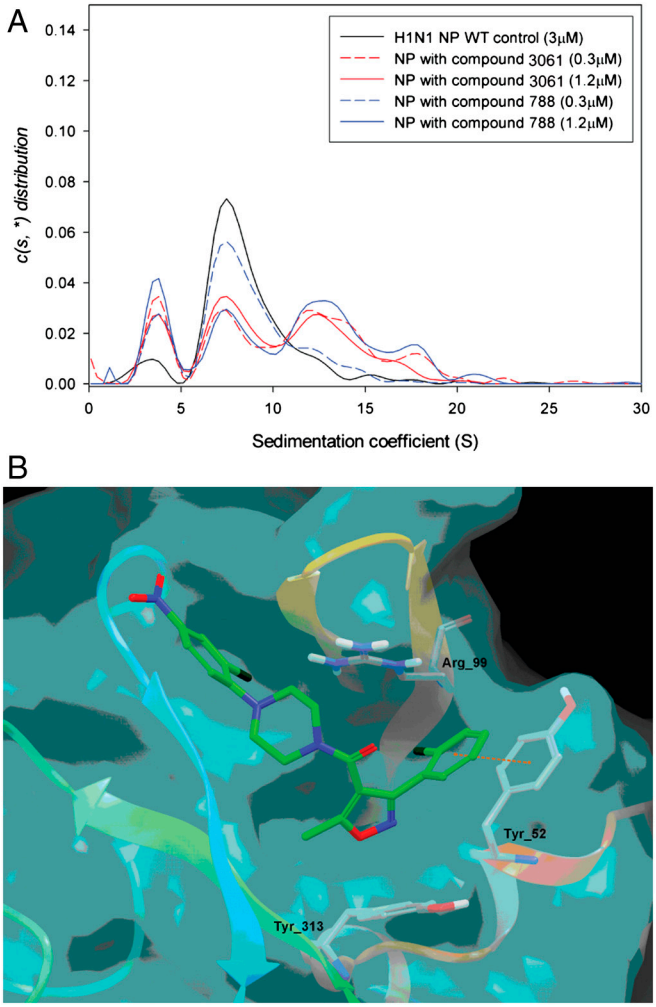

Fig. S8. Molecular basis of the effects of **3061** (FA-2) and **788** (Nucleozin). (*A*) Analytical ultracentrifuge analyses indicate that binding of the compounds leads to severe aggregation of the wild-type NP protein by either **3061** (FA-2) or **788** (Nucleozin). (*B*) Modeling of the molecular interaction of NP protein and **3061** (FA-2). Molecular modeling was done as described in *SI Materials and Methods*. Compound **3061** (FA-2) could form a pi-pi stacking interaction with NP at Y52. Another possible stacking interaction could occur between the compound's ring amide and NP Y313.

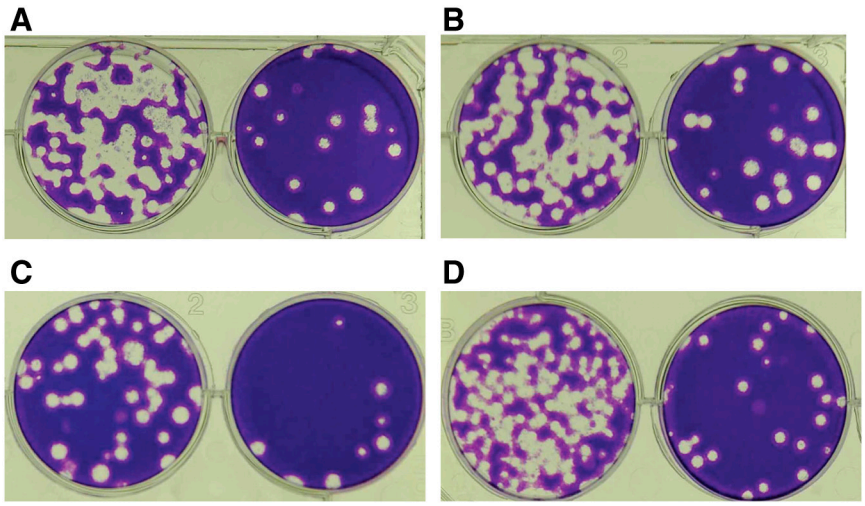

Fig. S9. Plaque appearance of isogenic recombinant influenza viruses with different NP point mutations. (*A*) WSN parental NP, (*B*) NP with Y52H, (*C*) NP with Y289H, and (*D*) NP with Y52H and Y289H.